Integration of range and image data for building reconstruction

Integration of range and image data for building reconstruction

F. Nex[a], F. Remondino[a], F. Rinaudo[b]

[a]3D Optical Metrology, Fondazione Bruno Kessler, Via Sommarive 18, 38122 Trento, Italy
<franex, remondino>@fbk.eu, http://3dom.fbk.eu
[b]Dept. of Land, Environment and Geo-Engineering , Politecnico di Torino, C.so Duca degli Abruzzi 24, 10121 Torino, Italy <fulvio.rinaudo@polito.it>

ABSTRACT

The extraction of information from image and range data is one of the main research topics. In literature, several papers dealing with this topic has been already presented. In particular, several authors have suggested an integrated use of both range and image information in order to increase the reliability and the completeness of the results exploiting their complementary nature. In this paper, an integration between range and image data for the geometric reconstruction of man-made object is presented. The focus is on the edge extraction procedure performed in an integrated way exploiting both the from range and image data. Both terrestrial and aerial applications have been analysed for the façade extraction in terrestrial acquisitions and the roof outline extraction from aerial data. The algorithm and the achieved results will be described and discussed in detail.

Keywords: integration, multi-image, range data, building extraction, terrestrial, aerial

1. INTRODUCTION

The extraction of precise and dense point clouds is nowadays possible using both LiDAR and image matching techniques. Nowadays, LiDAR and photogrammetric point cloud can indeed be considered comparable in most cases in terms of density and accuracy, as asserted in several papers both in terrestrial [1, 2] and aerial applications [3, 4, 5].

In typical mapping applications, once a point cloud (usually several millions of points) has been extracted, only the first (and shortest) part of the work has been completed. It is afterward required to process them in order to extract metric information (such as shapes, surface normal vectors, dimensions, polylines, etc.) of different objects (façades, buildings, streets, etc.) necessary to achieve the final product (3D model, drawing, thematic map, etc.). In some way, the classification, segmentation, modelling and in general the "understanding" of an unstructured point cloud in an almost automated way and without loss of accuracy is the real challenge to be faced nowadays by the research community. In the literature several papers deal with such topics: some contributions considered as input data only images [6, 7], others considered range data [8, 9, 10, 11, 12] and a growing number of papers rely on the integration of different data sources [13, 14, 15] and in particular from both range and image data [16, 17, 18, 19, 20, 21,22,23]. The single-technique approaches usually provide good results in very specific applications, while they are unable to be adapted to operative conditions far from their original use. On the other hand, the multi-technique solutions seem to be more versatile and able to achieve good results for a wider range of applications exploiting the complementary nature of range and image data. In particular, the integration of range and image data has shown promising results both in terrestrial and aerial applications for 3D modeling and mapping purposes [16, 17, 20, 24, 26] with a great improvement for façade modelling [27]. Generally the main problem is the correct extraction and 3D reconstruction of continuous and reliable edges. A complete edge extraction allows indeed to reconstruct the geometry of the surveyed objects in a better way [26, 28].

In this paper, a different edge extraction approach is presented. Assuming to have, for a defined area of interest, a point cloud (from range sensors or image matching) and a set of images, an integrated methodology is applied in order to retrieve the main geometric discontinuities of the scene which are the base for successive drawing or mapping purposes. Range sensors generally suffer in measuring the scene edges. On the other hand, despite edges are clearly measurable in the images, automated matching algorithms are generally not tailored to extract edges but they are matched only as integration to other image primitives. Therefore the proposed method extracts a set of reliable and continuous edges combining the available point cloud and images. The main goal is to obtain only the edges strictly requested in the

geometric reconstruction of the surveyed scene. A data driven approach is used in order to keep the maximum flexibility and detect discontinuities of generic shape. The final results show a more complete 3D reconstruction of man-made objects. The reported case studies are related to objects, both in terrestrial (building façades) and aerial acquisitions (roof outlines).

In the following section a brief overview of the workflow is given with the integrated edge extraction step presented more in detail in Section 3. Then, the first achieved results in the 3D object reconstruction will be shown. Finally, conclusions and future developments will be discussed.

2. ALGORITHM OVERVIEW

The proposed algorithm processes image and range information to extract geometric primitives useful for a complete and detailed reconstruction of man-made objects like building façades or roofs. A point cloud provided from dense image matching or range sensors (aerial or terrestrial) is used to drive the edge extraction and the matching process. In this way the geometric object boundaries, useful in speeding up the drawing production or the building modelling are determined. This approach has been already presented in [26, 28], where an exhaustive description of the algorithm is reported. In the following sub-sections the algorithm steps are briefly described (Figure 1), while the improvements developed in the edge extraction phase will be presented in the Section 3. The entire method, which starts from a dense and accurate point cloud and a set of images, is divided in blocks with concatenated processing steps.

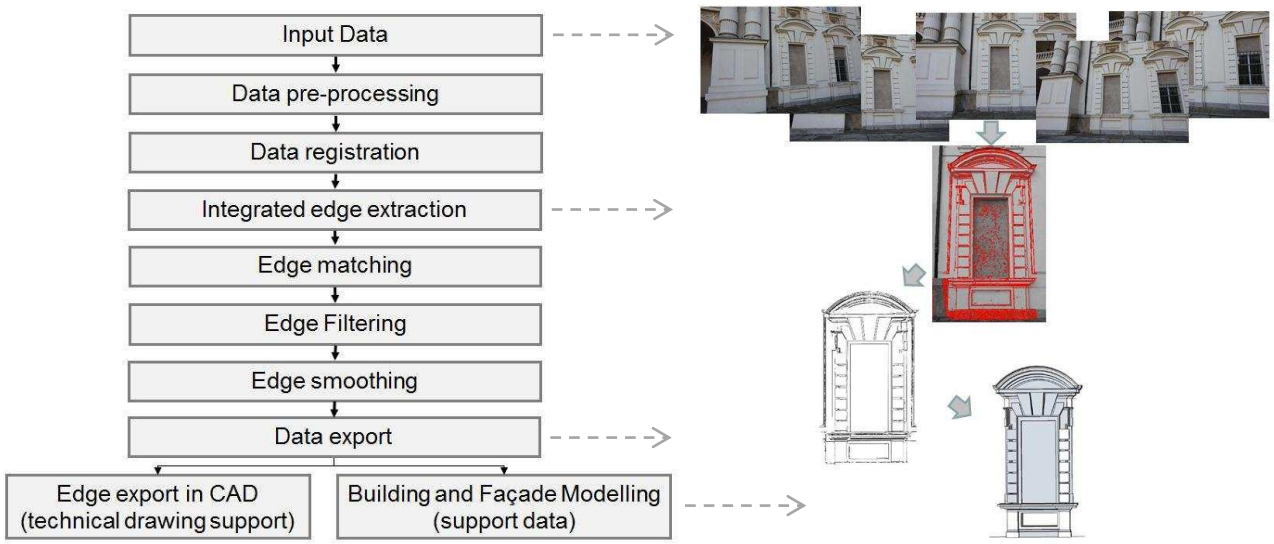

Figure 1. Workflow of the algorithm.

Data acquisition. Both in terrestrial and aerial applications the multi-image approach is recommended as it allows to improve the quality of the image matching results [29, 37]. In terrestrial applications, a set of convergent images or acquired according to an ad hoc network geometry is suggested. In the aerial case, high overlaps between images and adjacent strips are mandatory. High image resolution is always requested too: the extraction of building boundaries from images is complicated if low resolution images are used, as edges are usually blurred and irregular. The most central image of each set of images is considered as reference in the following matching process: when image sequences are available, different reference images are chosen in a proper way to assure a multi-view geometry.

Data pre-processing. In order to improve the edge extraction, a non-linear Edge Preserving Smoothing (EPS) filter [28] is applied to smooth the little radiometric variations but preserving and enhancing the main geometric discontents in the image. The boundaries of man-made objects are thus sharpened and smoothed deleting little radiometric changes that usually affect negatively the extraction of such elements [26]. Moreover, in order to improve the radiometric contents of all the images and achieve better matching results, the Wallis filter [31] is applied.

Data registration. Image orientation can be performed using different approaches [32, 33, 34]. Images and range data have to be already oriented in the same photogrammetric reference system. This process is not necessary if the available point cloud is generated with image matching techniques. Otherwise, the point cloud need to be co-registered in the photogrammetric reference system by means of a spatial roto-translation.

Integrated edge extraction. The integrated edge extraction is performed on a reference image, as described more in detail in following section. The final goal is to define only some "dominant" points able to provide a good approximation of the edge shape for its reconstruction in the matching process. The dominant points are recorded and linked by straight edges. The edges are extracted only in the regions of interest while areas where mismatches and blunders could occur are excluded with a manually masking approach.

Edge matching between images. A multi-image matching algorithm has been set up. This process can be divided in three steps. The first step is a modification of the Multi-Image Geometrically Constrained Cross Correlation ($MIGC^3$) proposed in [29]. Using a $MIGC^3$, the dominants points of each edge are matched in all the images in order to reconstruct the breakline positions in 3D (object space). The images are preliminarily undistorted (using the camera calibration data) in order to ease them into a central perspective and speed up the following processes. The $MIGC^3$ is able to match a high percentage of the extracted dominant point. Nevertheless, more than one reliable homologous point can be possible if only high cross correlation values are considered. A relational matching technique has been developed in order to solve these ambiguous matches and to improve the rate of the successfully matched points by means of a probability relaxation [35, 36]. The method uses the already matched dominants points as "anchors" and defines, in an iterative way, the more suitable match between candidates imposing a smoothing constraint. Finally, a Multi-Photo Least Square Matching[37] with the epipolar constraint has been performed for each extracted point to improve the accuracy up to a sub-pixel dimension.

Edge filtering. Once a set of 3D edges has been created, possible blunders are deleted using a filter that considers the reciprocal point positions on the same edge: the position of a point is "predicted" considering the neighbouring dominant points of the edge and then the difference between the predicted and real position of the point is evaluated. If the difference value is higher than a threshold, the point is delete. This filter works well if the blunders are isolated from each other. Then, more robust filter can be used to correct the edges when several blunders are close together: this algorithm uses the point cloud to verify the correctness of each dominant point: when it is farther than a threshold from the point cloud, the point is deleted.

Edge smoothing. The edges extracted by the image matching algorithm are random noise affected and they cannot be directly used in the drawing production or in the segmentation process. For this reason, a smoothing is needed in order to define a regular shape of the object, easing the edges in lines and curves. The great majority of edges in both close range and aerial applications can be classified in sets of lines and second order curves. Therefore, each edge must be split in different basic entities that describe its linear or curved parts separately and, each separate basic entity is simplified in lines and curves fitting the dominant point information with a robust least square approach.

Edge exporting. Geometric edges are exported in CAD environments in order to give a good preliminary data for the graphic drawing realization of the survey or to be used as additional information in the segmentation and modelling processes [27].

3. INTEGRATED EDGE EXTRACTION

The integrated edge extraction considers the range and image information in order to improve the continuity, length and reliability of the reconstructed edges in correspondence or in the closeness of only geometric discontinuities. As the conditions are very different in terrestrial and aerial acquisitions and the typology of objects to be detected is different too, two methods are used. In terrestrial applications, the goal is the detection of the geometric discontinuities of different shapes on the façade, while in aerial applications the building outlines and rooftops have to be detected. In both cases, the use of a model based approach is not flexible enough to correctly describe all the geometric discontinuities of a generic object. The common idea of these approaches is to reduce the regions where the edge extraction is performed using the range information. Edges are detected on the range data and then they are projected on the image defining a region of interest. In this way, the edges due to radiometric variations or shadows are almost completely ignored and only regions of the image in correspondence of geometric discontinuity are considered.

3.1 Edge extraction on terrestrial images

The completeness of the edge extraction process depends on several factors such as illumination condition, image resolution and typology of object. According to these factors, the edge extraction can produce fragmented or incomplete edges that reduce the quality of the achieved information. For this reason, using a standard edge extractor on an image, produces usually incomplete results. This problem can be partially solved decreasing the thresholds of the edge extractor (i.e. Canny operator), but this normally brings to an increase in the number of edges due to simple radiometric variations or shadows. The proposed approach try to solve these problems with a combined strategy. On one hand, the search area of edge extraction is reduced to the regions where a geometric discontinuity occurs; on the other hand, the completeness of the extraction is improved by locally decreasing the edge extraction thresholds. The algorithm works according to several steps:

- the available range information is firstly regularized in order to define a depth image of the scene simplifying the successive computation steps. The regularization procedure, which considers the range information as 2.5D data, depends on the range data density and detail dimensions (generally a 0.02-0.03 m step is used).

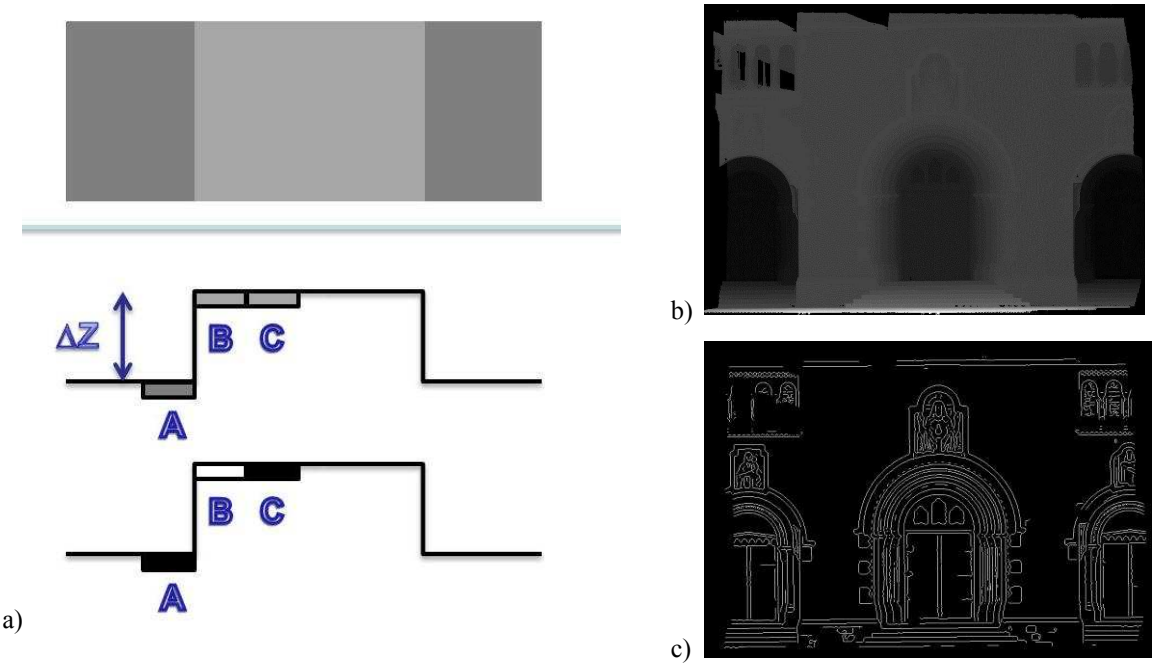

Figure 2. The principle of the breakline extraction (a) on the regularized depth image (b) with the achieved result (c).

- the geometric breaklines are extracted from the regularized range data (depth image) considering the gradients between adjacent pixels. A shown in Figure 2, the gradient between point A and B is very different from the gradient between B and C, thus point B can be considered a breakpoint. This process is repeated both for each point of the depth image in horizontal and vertical direction and the final result is a map of the geometric breaklines from the range data.

- the breaklines detected on the depth image can be projected onto the oriented images. In this way, an interest region is defined in the image space and the edge extraction can be performed only in this area. The Canny's operator [37] thresholds are stressed in order to preserve the edge continuity: in particular the lower threshold of the Canny's algorithm is further reduced in order to preserve the continuity between stronger edge points.

- the edges extracted with the Canny's operator are approximated considering each point where the edge changes its curvature as a dominant point, and linking with a straight line the points comprised between two adjacent dominant points. A more detailed description of the algorithm is given in [27].

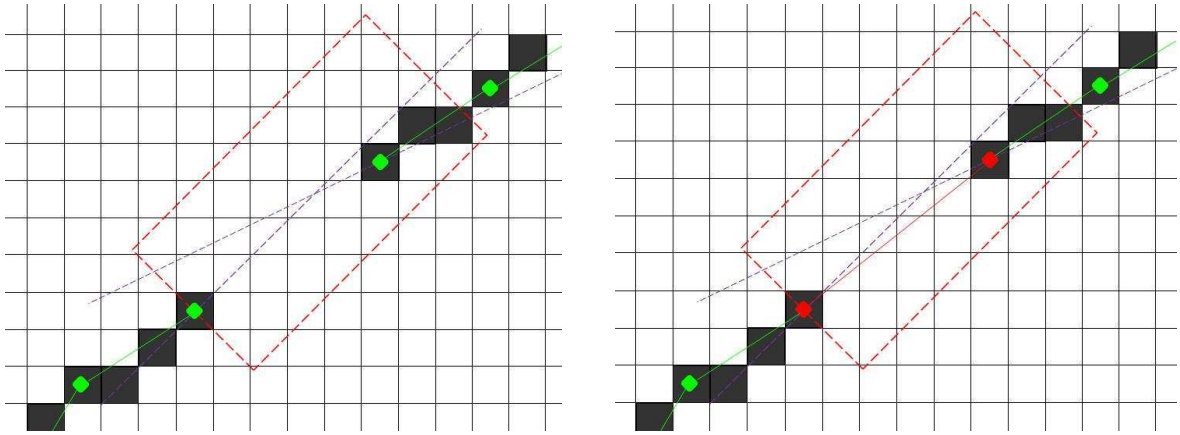

(a) (b)

Figure 4. Edge merging process: the red box define the bounding box for the merging process; violet lines defines the edge direction in correspondence of the extremes (red points).

- although the Canny's thresholds are used in an adaptive mode, several edges can be divided or incomplete, thus requiring an aggregation strategy, in particular for long edges. The direction of the edge in correspondence of the extreme is computed considering the last four dominant points of the edge. According to this direction a bounding box is defined and the presence of other edge extremes is looked for (Figure 4a). When another extreme is found and the direction of the other edge extreme is similar, the edge is merged (Figure 4b). The edges can be successfully merged only if the missing part of the edge is limited to few pixels. Wrong merges can be generated if the bounding box is too big: the maximum bounding box dimensions varies according to the complexity of the façade and the quality of the image.

3.2 Edge extraction on aerial images

Aerial acquisitions over a urban area usually considers 3 main classes of objects: ground (bare soil, grass, road, sidewalk, etc.), buildings and vegetation (i.e. trees). For this reason, the classification of building regions from range and image data is performed before the outlines and rooftop extraction. Several building extraction algorithms have been already proposed, considering LiDAR data, multispectral images or maps as input data [11, 13, 39, 40,41]. Nevertheless, in this paper simple RGB images and "single return" DSM (generated by LiDAR or image matching techniques) are used. Only some approaches considered the rooftops detection and reconstruction on the buildings [15, 22] but they rely on very dense point clouds.

A two-step integrated method has been implemented. In the first step the buildings outline and rooftop approximate positions are detected on the range data. Their position is then refined by means of edge extraction on the images, as point clouds are unable to define the precise roof breakline positions.

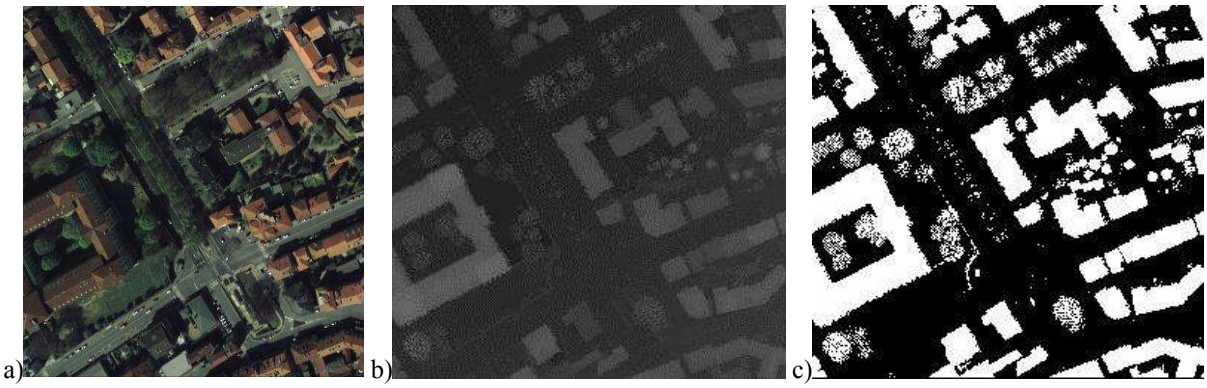

a) b) c)

Figure 5. (a) original image; (b) regularized DSM (c) off-ground extraction over the same area.

Off-ground data is formerly extracted from the data using the regularized range data (Figure 5). The simple assumption is that the height of a ground is lower than the heights of neighbouring non-ground points. In the literature, several methods for the off-ground points classification are reported [16, 17, 39, 40]. In the proposed method the ground filtering is performed through an iterative regular grid filtering. This approach consider two different problems: (i) the ground height variations over a big region patch and (ii) the presence of big dimensions buildings that avoid to determine the ground height if a too little DSM patch is considered. For these reasons, the ground height is iteratively computed on different DSM patch dimensions: the most representative value of the ground height is determined considering the minimum height value [39] on the different dimension DSM patches. Off-ground points are defined considering points higher than a defined threshold (2.5-4 m) the ground height value. This approach has shown to be reliable when the terrain slope increases too.

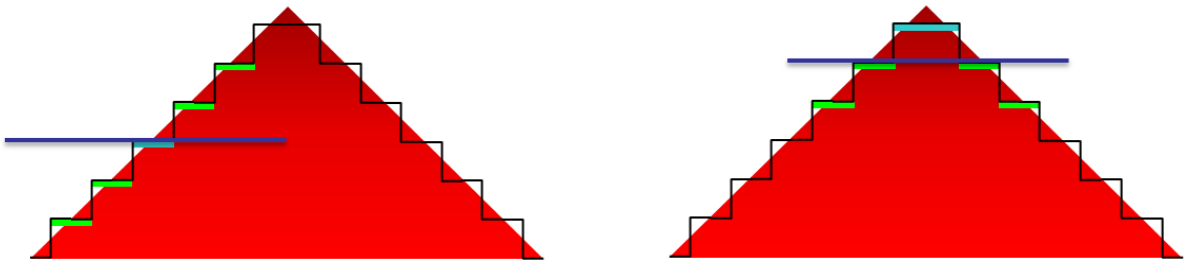

(a) (b)

Figure 6. Rooftop detection by means of "reverse median filtering".

The building terrain is then extracted from the off-ground data filtering the vegetation. To do that, the local height variability of the points is considered, as this value is higher in correspondence of vegetated areas than over manmade objects [36]. In the proposed approach an area of 5 by 5 meters is considered and the standard deviation and the difference between maximum and minimum values are evaluated.

Building outlines are detected using the height gradients as already described in Section 3.1. As this approach is not sensitive enough to determine the rooftops of every building, they are extracted from the building region by means of a "reverse" median filtering. The median height value of a 5 by 5 patch is computed for each pixel on the building region and this value is compared to the central pixel height value. As shown in Figure 6, this difference is maximum in correspondence of rooftops and it is possible to extract the region where rooftops lies.

The results achieved in in the building filtering are shown in Figure 7a while the detected rooftops are shown in Figure 7b. The above presented algorithm allows the building geometric elements to be defined reducing the edge extraction on the images as presented in Section 3.1.

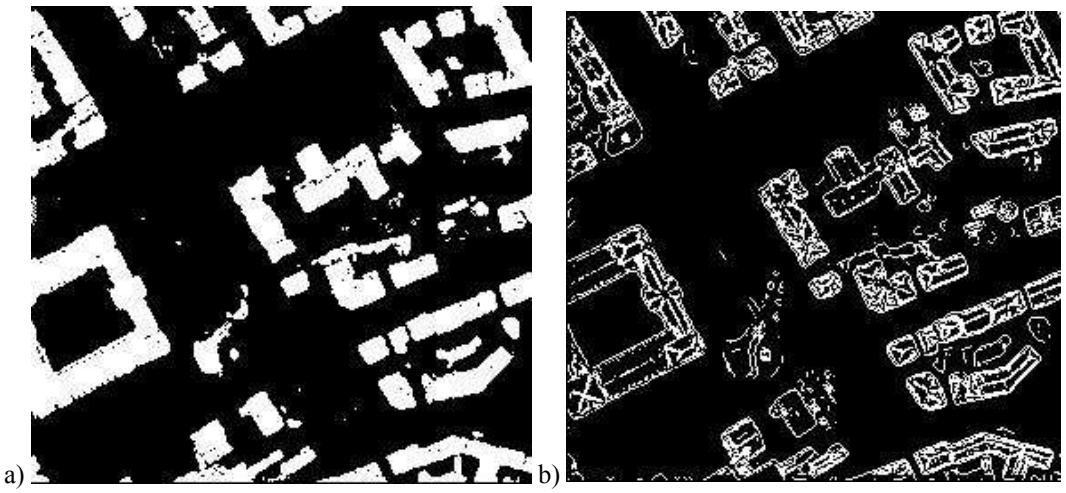

a) b)

Figure 7. Example of building regions (a) and approximate outline and rooftop regions (b).

4. TESTS AND ACHIEVED RESULTS

In the following, the first results on both terrestrial and aerial images will be presented. Two different terrestrial tests have been realized: the first test considered low resolution images to evaluate the performance of the proposed algorithm in extreme conditions, while the second one was performed on high resolution images. The aerial test was finally performed on a dense urban area over the city of Torino (Italy).

4.1 Results from terrestrial images

The first terrestrial test was performed on a set of convergent images (available as ISPRS Commission III dataset). The image resolution is 6 Mpixel, while the taking distance was about 15 m: a GSD on the building façade was about 6 mm. A dense range data was available on the same area acquired with a terrestrial laser scanner instrument. The edges on the image were blurred and their completeness after the edge extraction was reduced. Several radiometric variations due to shadows or colour variations were visible on the façade. The range data was regularize as shown in Figure 8a and the geometric breakline was extracted from this data using the approach presented in Section 3.1. A 0.02 m height gradient was considered in the edge extraction from the range data.

a) 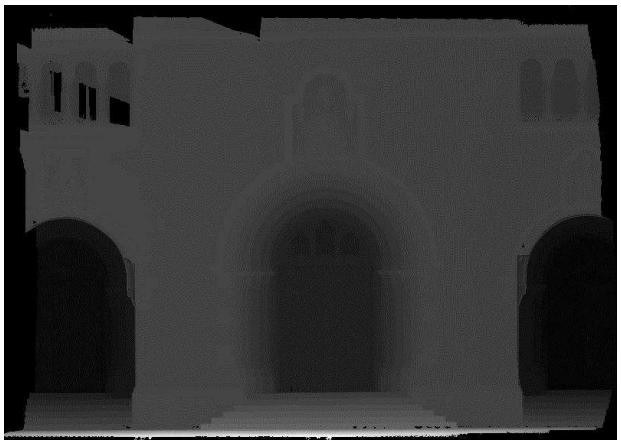 b) 

Figure 8. Regularized DSM (a) and corresponding region of interest for the edge extraction procedure (b).

Thanks to this information it is possible to limit the area of interest of the edge extraction on the reference image (Figure 8b) and push the Canny's operator thresholds in order to increase the completeness of the process in these areas. The completeness of edges was finally increased by merging the neighbouring edges and deleting the edges that are short and curved. The final result is shown in Figure 9.

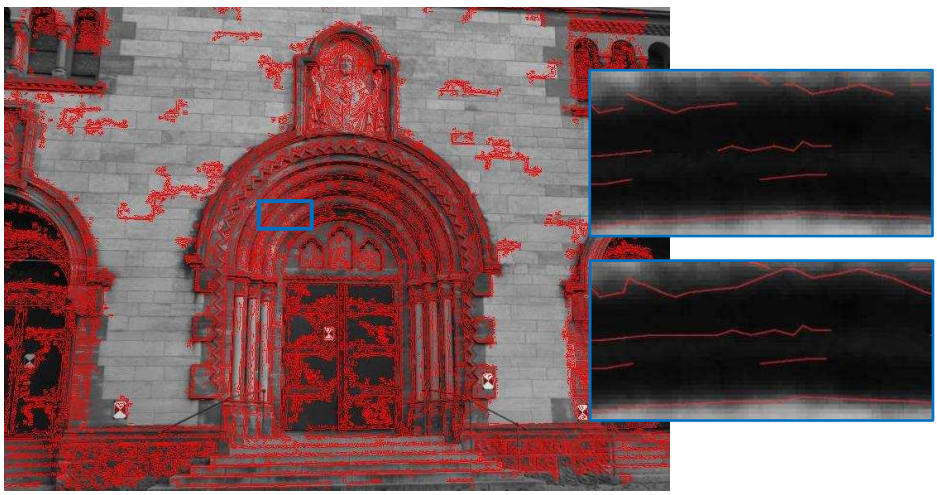

Figure 9. Edges after the merge process: example of edge before (upper) and after (lower) the merging process.

Due to the low resolution of the available images, the edge extraction was far from reaching a complete result and some of the geometric discontinuities of the scene were not completely extracted while some useless data were still present. The extracted edges were finally matched, filtered and finally smoothed according to the approach presented in Section 2. The recovered 3D edges are shown in Figure 10.

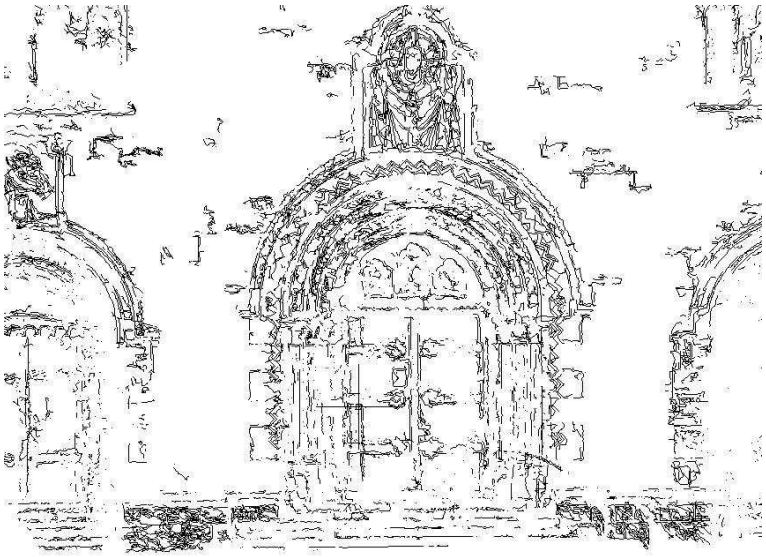

Figure 10. Edges exported in CAD

When a higher resolution set of images is available, the extraction procedure obtains more reliable and complete results. A second test was performed on 5 images (GSD ca 2 mm) acquired on a corner of an historical building of Torino (Italy). With such images the integrated edge extraction improves the completeness of the achieved information merging edges that can be divided or separated.

a) b) c)

Figure 11. Regularized DSM (a), corresponding region of interest (b) and extracted edges (c).

In Figure 11 the geometric discontinuities detected on the range data and the corresponding edges extracted on the reference image are shown. These edges were finally matched, filtered and smoothed, achieving the results shown in Figure 12.

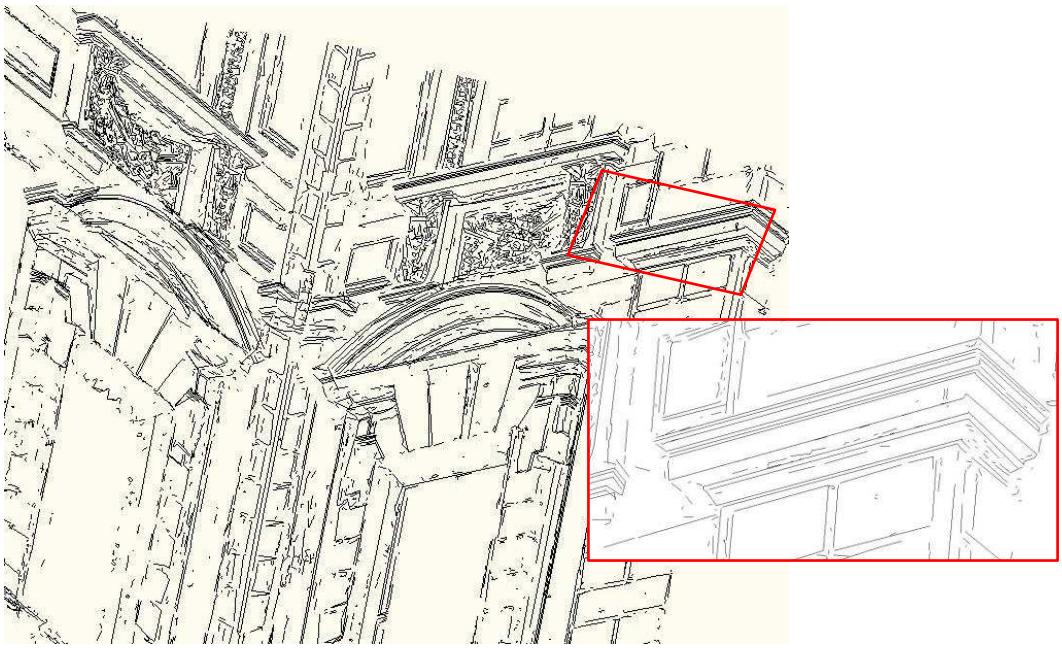

Figure 12. 3D edges exported in cad.

4.2 Results from aerial images

The dataset contains 6 aerial images (DMC Z/I Imaging-Hexagon Geosystems, GSD=12 cm) and 1m regular spacing DSM (single return) over a urban area of Torino (Italy). The test area (ca 0.5x0.5 km) is characterized by several high buildings, trees and variation of the ground height (Figure 13).

Figure 13. An aerial image over the test area.

From the available DSM, the buildings were extracted according to the algorithm described in Section 3.2. In order to filter the ground, variable box regions from 60 to 30 m were considered and an height threshold of 3.5 m for the off-ground filtering was fixed. Then the trees were filtered according to the algorithm described in Section 3.2. The result (Figure 14) is complete and correct even if some problems still remain where the vegetation is very close to buildings, as shown in the lower right part of the figure. In these conditions some trees are still classified as buildings.

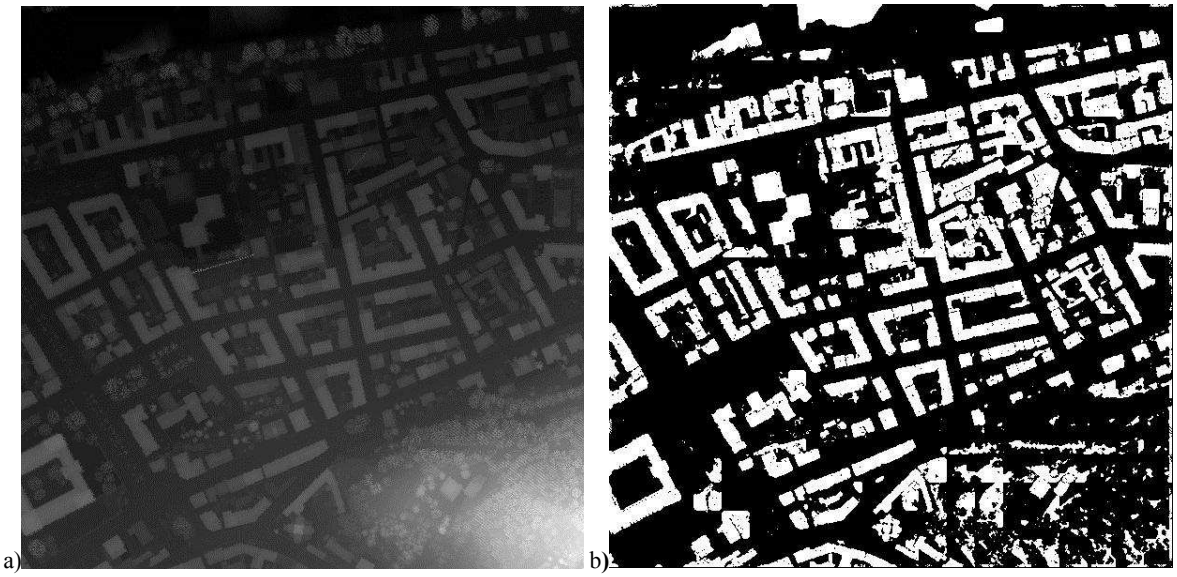

Figure 14. Regularized DSM (a) and extracted building regions (b).

The building rooftops and outlines were finally extracted on the same area achieving the result shown in Figure 15a. It can be noted that the results are complete and the areas of interest on the buildings are correctly detected. The regions detected in Figure 15a were projected in the reference image to limit the edge extraction. The edges extracted on the image were finally filtered to delete the ones jagged and shorter than 15 pixels. The achieved result is shown in Figure 15b.

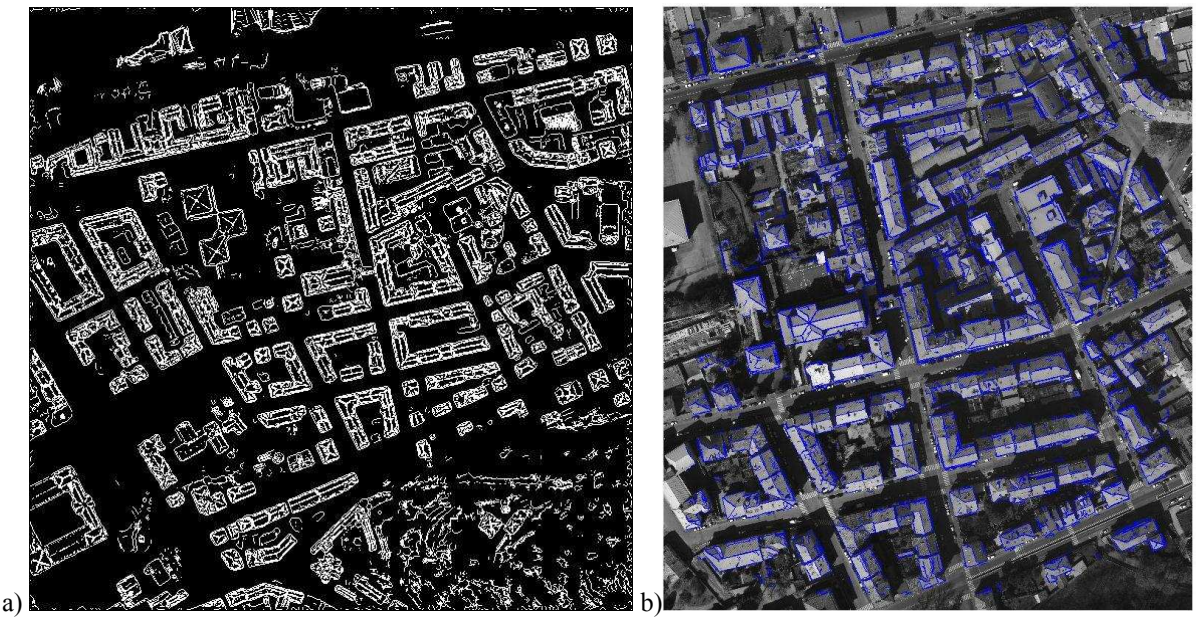

Figure 15. Region of interest for the edge extraction on the test area (a) and extracted edges on part of the analyzed test site (b).

Most of the building outlines and rooftops were correctly detected. Few lines are missing in correspondence of bad textured areas, but the number of useless points on the roofs and in proximity of buildings was reduced thanks to the filtering of the edges. The merging of adjacent edges improved the completeness of the result. The extracted edges were finally matched and smoothed according to the workflow described in Section 2. The final 3D result is shown in Figure 16.

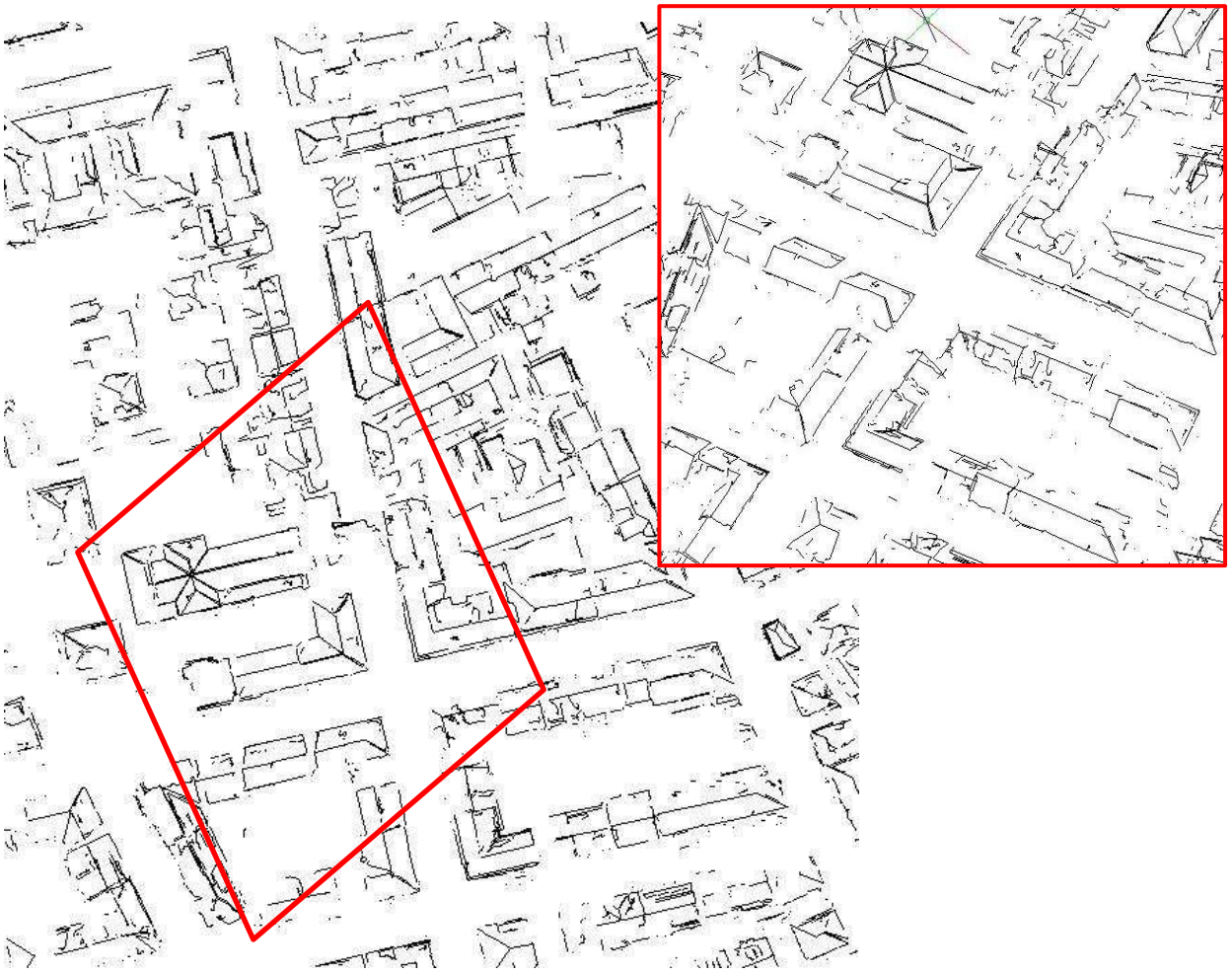

Figure 16. 3D edges exported in CAD.

The reported results, if compared to a former tests [26] on the same area, show a huge improvement thanks to the integrated edge extraction that allowed to delete before the matching process the useless edges in correspondence of shadows and radiometric variations, increasing the completeness of the 3D product.

5. CONCLUSIONS

In this paper an improved integrated approach for edge extraction from terrestrial and aerial images have been shown. The method exploits both range and image information in order to provide for reliable and complete 3D edges useful for mapping and drawing purposes. The presented approach could complete the information provided by a LiDAR point cloud, that is generally unable to define the precise position of object breaklines and usually smooth the geometries of the surveyed objects. The proposed method gives also a complementary information with respect to dense matching

algorithms as the extracted edges are concentrated in proximity of object breaklines and they are usually longer and more reliable.

The achieved results have shown how the edge extraction can be still critical especially in terrestrial applications. The use of low resolution images or poor GSDs make the edge extraction more difficult and unreliable, delivering incomplete and very noisy edges. The integrated edge extraction presented in this paper partially solves this problem as incomplete results are still visible. The height gradient in the edge extraction from range data is still critical: low values provide incomplete results, while too high values increase the number of useless data. Then the merging of adjacent edges is still insufficient to reconstruct and complete edge extraction process when the edge missing parts are long. For these reasons a good image resolution is strictly recommended.

The aerial test has underlined the improvement that the integrated edge extraction provide to the final result. The feature extraction from the range data allows to detect the buildings outlines and rooftops in a complete way, reducing and easing the following edge extraction on the image. Then the edges are successfully filtered exploiting their geometric properties, i.e. their straightness and length. At the end of this process, approximately the 90% of building outlines has been detected on the images. Finally, the matching process and the smoothing allow to deliver more complete 3D edges.

In the future work the integrated edge extraction has to be improved especially in terrestrial applications. The edge extraction is still conditioned by the presence of local edge variations that influences the smoothness and the completeness of the edge. On the other hand, the geometric breaklines are usually smooth and complete defining the correct local direction of the edge. This local direction could be exploited in the edge extraction on the image, defining a preferential direction of search of edges on the image in that direction. In this way, the smoothness and the completeness of the edge extracted on the image are expected to increase. Then a topological analysis of the extracted edges will be developed to check the correctness and the completeness of the extracted edges.

The completeness of edges must be improved in aerial applications too as some lines are missing or incomplete. Several modifications will be implemented on the matching algorithm, especially the relational matching algorithm that sometimes does not succeed in the ambiguity solving during the matching process. Then, some edges give redundant information (Figure 17) such as parallel lines in correspondence of the rooftop and the outlines while other lines are missing. For this reason a topological analysis of each roof will be realized in order to complete and improve the roof reconstruction.

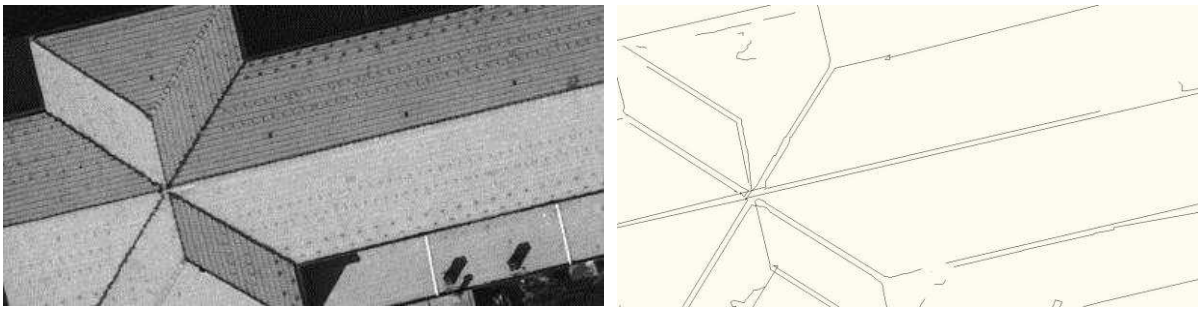

Figure 17. Example of parallel lines extracted from an aerial image.

REFERENCES

[1] Remondino, F., El-Hakim, S., Gruen, A., Zhang, L., "Turning images into 3D models," IEEE Signal Processing Magazine 25(4), 55-64 (2008).

[2] Hiep, V.,H., Keriven R., Labatut, P., Pons J-P., "Towards high resolution multi-view stereo," Proc. Computer Vision and Pattern Recognition, 1430-1437 (2009).

[3] Paparoditis, N., Souchon, J-P. Martinoty, G., Pierrot-Deseilligny, M., "High-end aerial digital cameras and their impact on the automation and quality of the production workflow," ISPRS Journal of Photogrammetry & Remote Sensing 60, 400-412 (2006).

[4] Hirschmüller, H., "Stereo processing by semi-global matching and mutual information," IEEE Transactions on Pattern Analysis and Machine Intelligence 30(2), 328-341 (2008).

[5] Gehrke, S., Morin, K., Downey, M., Boehrer, N., Fuchs, T., "Semi-global matching: an alternative to LiDAR for DSM generation?," International Archives of Photogrammetry and Remote Sensing and Spatial Information Sciences - Canadian Geomatics Conference XXXVIII(1), (2010).

[6] Trias-Sanz, R., Stamon, G., Louchet, J., "Using colour, texture, and hierarchical segmentation for high resolution remote sensing," ISPRS Journal of Photogrammetry & Remote Sensing 63, 156-168 (2008).

[7] Zebedin, L., Klaus, A., Gruber-Geymayer, B., Karner, K., "Towards 3D map generation from digital aerial images," ISPRS Journal of Photogrammetry & Remote Sensing 60, 413-427 (2006).

[8] Habib, A. F., Chang, Y-C., Lee D. C., "Occlusion-based methodology for the classification of LiDAR data," Photogrammetric Engineering & Remote Sensing 75(6), 703-712 (2009).

[9] Matikainen, L., Hyyppä, J., Kaartinen, H., "Comparison between first pulse and last pulse laser scanner data in the automatic detection of buildings," Photogrammetric Engineering and Remote Sensing 75(2), 133–146 (2009).

[10] Sampath, A., J. Shan, "Building Reconstruction from Airborne LiDAR Data Based on Clustering Analysis," Proc. International Society for Photogrammetry and Remote Sensing Congress, (2008).

[11] Dorninger, P., Nothegger, C., "3D segmentation of unstructured point clouds for building modelling," Proc. PIA - Photogrammetric Image Analysis, (2007).

[12] Pu, S., Vosselman, G., "Knowledge based reconstruction of building models from terrestrial laser scanning data," ISPRS Journal of Photogrammetry and Remote Sensing 64, 575-584 (2009).

[13] Demir, N., Poli, D., Baltsavias, E., "Detection of buildings at airport sites using images & LiDAR data and a combination of various methods," International Archives of Photogrammetry and Remote Sensing and Spatial Information Sciences XXXVIII(3/W4), 71-77 (2009).

[14] Sohn, G., Dowman, J., "Data fusion of high-resolution satellite imagery and LiDAR data for automatic building extraction," ISPRS Journal of Photogrammetry and Remote Sensing 62, 43-63 (2007).

[15] Vosselman, G., "Fusion of laser scanning data, maps, and aerial photographs for building reconstruction," IGARSS '02 Geoscience and Remote Sensing Symposium 2002 IEEE International, 85-88 (2002).

[16] Awrangjeb, M., Ravanbakhsh, M., Fraser, C.S., "Automatic detection of residential buildings using LiDAR data and multispectral imagery," ISPRS Journal of Photogrammetry and Remote Sensing 65, 457-467 (2010).

[17] Habib, A.F., Zhai, R., Kim, C., "Generation of complex polyhedral building models by integrating stereo aerial imagery and LiDAR data," Photogrammetric Engineering & Remote Sensing 76, 609-623 (2010).

[18] Kock, M., Kaehler, M., "Combining 3D laser-scanning and close range photogrammetry – An approach to exploit the strength of both methods," Proc. CAA 2009 Computer Application to Archaeology, 1-7 (2009).

[19] Rottensteiner, F., Trinder, J., Clode, S., Kubik, K., "Fusing airborne laser scanner data and aerial imagery for the automatic extraction of buildings in densely built-up areas," ISPRS Journal of Photogrammetry & Remote Sensing 62, 135-149 (2007).

[20] Boehm, J., Becker, S., Haala, N., "Model refinement by integrated processing of laser scanning and photogrammetry," Proc. 2nd ISPRS International Workshop 3D-ARCH 2007: "3D Virtual Reconstruction and Visualization of Complex Architectures" XXXVI-5/W47, CD-ROM (2007).

[21] Alshawabkeh, Y., [Integration of laser scanning and photogrammetry for cultural heritage], PhD Thesis Institut für Photogrammetrie der Universität Stuttgart, (2006).

[22] Bretar, F., Roux, M., "Hybrid image segmentation using LiDAR 3D planar primitives," Proc. Laserscanning 2005, 72-78 (2005).

[23] Habib, A.F., Ghanma, M.S., Tait, M., "Integration of LiDAR and photogrammetry for close range applications," International Archives of Photogrammetry, Remote Sensing and Spatial Technology and Spatial Information Sciences XXXIV(3), (2004).
[24] Nakagawa, M., Shibasaki, R., "Study of making city modelling image and laser range data," Proc. 22nd Asian Conference on Remote Sensing, (2001).
[25] Nex, F., Rinaudo, F., 2009, "New integration approach of photogrammetric and LiDAR techniques for architectural surveys," Proc. Laserscanning 2009, 12-17 (2009).
[26] Lingua, A., Nex, F., Rinaudo, F., "Integration of airborne laser scanner and multi-image techniques for map production," Proc. SPIE Remote Sensing 7831, 14-28 (2010).
[27] Chiabrando, F., Nex, F., Piatti, D., Rinaudo, F. "Integration between calibrated time-of-flight camera data and multi-image matching approach for architectural survey," Proc. SPIE Remote Sensing 7830, (2010).
[28] Nex, F., [Multi-image matching and LiDAR data new integration approach], PhD Thesis, Politecnico di Torino, Torino (2010).
[29] Zhang, L., [Automatic Digital Surface Model (DSM) generation from linear array images], PhD Thesis, ETH Zurich, No. 16078, IGP Mitteilung N. 90 (2005).
[30] Lee, J.-S. , "Digital image smoothing and the sigma filter," Comput. Vis., Graph. Image Process. 24, 255–269 (1983).
[31] Wallis, R., "An approach to the space variant restoration and enhancement of images," Proc. Symposium on Current Mathematical Problems in Image Science, 329- 340 (1976).
[32] Barazzetti, L., Remondino, F., Scaioni, M., "Automated and accurate orientation of complex image sequences," International Archives of Photogrammetry, Remote Sensing and Spatial Information Sciences 38(5/W16) - 4th International Workshop 3D-ARCH 2011: "Virtual Reconstruction and Visualization of Complex Architectures", CD-ROM (2011).
[33] Pierrot Deseilligny, M., Clery, I., "APERO, an open source bundle adjustment software for automatic calibration and orientation of set of images," International Archives of Photogrammetry, Remote Sensing and Spatial Information Sciences 38(5/W16) - 4th International Workshop 3D-ARCH 2011: "Virtual Reconstruction and Visualization of Complex Architectures", CD-ROM (2011).
[34] Roncella, R., Re, C., Forlani, G., "Performance evaluation of a structure and motion strategy in architecture and cultural heritage," International Archives of Photogrammetry, Remote Sensing and Spatial Information Sciences 38(5/W16) - 4th International Workshop 3D-ARCH 2011: "Virtual Reconstruction and Visualization of Complex Architectures", CD-ROM (2011).
[35] Christmas, W. J., Kittler, J., Petrou, M., "Structural Matching in Computer Vision Using Probabilistic Relaxation," PAMI 17(8), 749-764 (1995).
[36] Hancock, E. R., Kittler, J. "Edge Labelling using Dictionary-based Relaxation," PAMI 12(2), 165-181 (1990).
[37] Baltsavias, E., [Multiphoto geometrically constrained matching], PhD Thesis, ETH Zurich, Switzerland, (1991).
[38] Canny, J., "A computational approach to edge detection," IEEE Trans. Pattern Analysis and Machine Intelligence, 679–714 (1986).
[39] Lee D.H., Lee K.M., Lee S.U., "Fusion of LiDAR and imagery for reliable building extraction," Photogrammetric Engineering & Remote Sensing 74(2), 215-225 (2008).
[40] Chen, L.C., Teo, T.A., Hsieh, C.H., Rau J.Y., "Reconstruction of building models with curvilinear boundaries from laser scanner and aerial imagery," Lecture Notes in Computer Science 4319, 24-333 (2006).
[41] Kim C., Zhai, R., Habib, A., "Complex digital building model generation through the integration of photogrammetric and LiDAR data," Proc. ASPRS 2009 Annual Conference, CD-ROM (2009).